Mon. Not. R. Astron. Soc. **361,** 1063–1076 (2005) doi:10.1111/j.1365-2966.2005.09263.x

A comparative analysis of empirical calibrators for nebular metallicity

Enrique Pérez-Montero★ and Angeles I. Díaz
Departamento de Física Teórica, C-XI, Universidad Autónoma de Madrid, 28049 Madrid, Spain

Accepted 2005 May 24. Received 2005 May 12; in original form 2004 September 3

ABSTRACT

We present a new analysis of the main empirical calibrators of oxygen abundance for ionized gas nebulae. With that aim we have compiled an extensive sample of objects with emission-line data including the near-infrared [S III] lines and the weak auroral lines which allow for the determination of the gas electron temperature. For all the objects the oxygen abundances have been derived in a homogenous way, using the most recent sets of atomic coefficients and taking into the account the effect of particle density on the temperature of O^+. The residuals between directly and empirically derived abundances as a function of abundance have been studied. A grid of photoionization models, covering the range of physical properties of the gas, has been used to explain the origin of the uncertainties affecting each abundance calibrator. The range of validity for each abundance parameter has been identified and its average uncertainty has been quantified.

Key words: ISM: abundances – H II regions.

1 INTRODUCTION

H II regions, from diffuse H II regions in the Galaxy to extragalactic H II regions (GEHR) and H II galaxies, have been for many years, the main source of information concerning metallicity in distant galaxies. Their bright emission-line spectra are visible in all kinds of objects where there have been recent episodes of star formation. The analysis of these nebular spectra constitutes the best method, if not the only one, for the determination of the chemical abundances of elements such as He, N, O, Ne, Ar, S having optical emission lines corresponding to different ionization states. An accurate knowledge of these abundances is essential for a complete understanding of the evolution of stars and stellar systems and has allowed some light to be shed on several questions concerning the chemical evolution of galaxies in the local Universe. They are now becoming even more relevant with the regard to the younger Universe.

Recombination lines yield the most accurate abundances because of their weak dependence on nebular temperature. In fact, helium abundances can be derived to an accuracy of better than 5 per cent. Unfortunately, most of the observed emission lines in ionized nebulae are collisionally excited and their intensities depend exponentially on temperature. In principle, this temperature can be determined from appropriate line ratios, the most widely used being that of [O III] $\lambda4363/(\lambda4959 + \lambda5007)$ although, recently, the improved sensitivity of new detectors in larger telescopes allows for the measurement of other auroral lines, which are less temperature sensitive (Kinkel & Rosa 1994; Castellanos, Díaz & Terlevich 2002a, hereinafter CDT02).

All of these ratios involve the detection and measurement of one intrinsically weak line which in many objects is too faint to be observed. This is the case for regions with a high metal content – where the efficient cooling exerted by metallic ions renders weak lines undetectable – H II regions in distant galaxies and objects with low surface brightness. In these cases, empirical methods based on the intensities of strong, easily observable, optical lines have been developed and are nowadays widely used.

The so-called 'empirical methods' are based on the cooling properties of ionized nebulae which ultimately translate into a relationship between emission-line intensities and oxygen abundance. In fact, when the cooling is dominated by oxygen, the electron temperature depends inversely on oxygen abundance. Since the intensities of collisionally excited lines depend exponentially on electron temperature, a relation is expected to exist between these intensities and oxygen abundances.

According to Pagel et al. (1979), under the assumptions that (a) the nebula is ionization bounded, (b) the region can be represented by small clumps of gas with a given electron density surrounded by much less dense material, so that the degree of ionization is proportional to $(\epsilon^2 n_e Q_H)^{1/3}$, where n_e is the clump electron density, Q_H is the number of hydrogen ionizing photons and ϵ is the filling factor and (c) the cooling is fixed by oxygen abundance, we can consider that the emission-line spectrum of the nebula will depend on: the energy distribution of the ionizing radiation field, the ionization parameter and the oxygen abundance. Therefore, if a single relation between the chosen calibrator and the oxygen abundance is sought, further assumptions are needed, implying that either the hardness of the radiation field or the degree of ionization or both depend on oxygen abundance.

Following these ideas, several abundance calibrators have been proposed involving different emission-line ratios: among others,

★E-mail: enrique.perez@uam.es

[O III] λ5007/Hβ (Jensen, Strom & Strom 1976; [O III] λ5007/[N II] λ6584 (Alloin et al. 1979) and ([O II] λ3727 + [O III] λ5007)/Hβ (R_{23}; Pagel et al. 1979). The advantages and drawbacks of the different calibrators have been discussed by several authors (see Pagel, Edmunds & Smith 1980; Kennicutt & Garnett 1996; Kewley & Dopita 2002). Although abundances derived through the use of these calibrations are recognized to suffer from considerable uncertainties, they are still believed by many authors to trace large-scale trends in galaxies. Empirical methods have been used to derive abundances in objects as different as dwarf irregular galaxies (e.g. Skillman, Kennicutt & Hodge 1989), individual H II regions in spiral galaxies (e.g. Oey & Kennicutt 1993), low surface brightness galaxies (McGaugh 1994), nuclear starbursts (e.g. Storchi-Bergmann, Calzetti & Kinney 1994) and even active galactic nuclei (Storchi-Bergmann et al. 1998). They have also been employed in the derivation of abundance distributions in the discs of spiral galaxies (e.g. Belley & Roy 1992; Van Zee, Skillman & Salzer 1998) and emission-line galaxies at intermediate redshift (e.g. Kobulnicky & Kewley 2004).

In this work we perform a comparative analysis of the principal empirical calibrations of abundances which are based on the intensities of the nebular lines of oxygen, nitrogen and sulphur, visible in the optical and far-red spectral regions. All of these calibrations present a considerable scatter, usually larger than that associated with observational errors and probably related to the assumptions mentioned above. The aim of our work is to understand the reasons for this scatter and, whenever possible, to find ways of improving the empirical derivation of abundances.

In order to do that, we have compiled a large sample of emission-line objects (H II galaxies, GEHR and diffuse H II regions in the Galaxy and the local group) with a direct determination of the total oxygen abundance through the measurement of the auroral lines of [O III] λ4363, [O II] λ7327 or [S III] λ6312 and we have constructed a complete sequence of photoionization models, covering the main physical properties of these objects.

In the next section we describe the sample of objects and the process of determination of the oxygen abundance. In Section 3, we summarize the main properties of the photoionization models used for our analysis which is then presented in Section 4. Finally, Section 5 summarizes our results and the main conclusions reached.

2 SAMPLE OF OBJECTS AND ABUNDANCE DERIVATION

Our sample is composed of a combination of different emission-line objects ionized by young massive stars: diffuse H II regions in the Galaxy and the local group (DHR), giant extragalactic H II regions (GEHR) and H II galaxies (HIIG), and therefore does not include planetary nebulae or objects with non-thermal activity. For all of them direct determinations of electron temperature exist, thus allowing the derivation of the oxygen abundance which we have taken as the observational metallicity indicator. The sample includes the objects analysed in Díaz & Pérez-Montero (2000, hereinafter DPM00) with the addition of low-excitation GEHRs from CDT02; GEHRs in M101 (Kennicutt, Bresolin & Garnett 2003) and M51 (Garnett, Kennicutt & Bresolin 2004); GEHRs in galaxies in the Sculptor Group (Skillman, Côté & Miller 2003) and the Virgo cluster (Vílchez & Iglesias-Páramo 2003); and H II galaxies from the works of Guseva, Izotov & Thuan (2000), Popescu & Hopp (2000) and Kniazev et al. (2001). Data from these latter objects have been complemented with information in the spectral range between 7000 Å and 1 μm from Pérez-Montero & Díaz (2003, hereinafter PMD03; 12 H II galaxies) and Garnett (1992; 13 objects), including the [S III] strong emission lines.

The sources for the line intensities, together with the number and class of the collected objects, are summarized in Table 1. The total sample comprises 367 objects with lines in the optical part of the spectrum, 282 of them with [N II] data and 126 with near-infrared (near-IR) [S III] data.

The physical conditions – electron temperature, electron density and oxygen abundance – for the whole sample have been recalculated using the same procedures as in PMD03, based on the five-level statistical equilibrium model in the task TEMDEN contained in the software package IRAF (De Robertis, Dufour & Hunt 1987; Shaw & Dufour 1995). The atomic coefficients used are the same as in PMD03 and are referenced in table 4 of that work. Electron densities were determined from the [S II] λ6717/λ6731 line ratio. Electron temperatures have been calculated from the [O III] (λ4959 + λ5007)/λ4363 line ratio for all but 13 objects of the sample for which the [S III] (λ9069 + λ9532)/λ6312 line ratio has been used instead. These latter objects are of low excitation and lie on the high-metallicity range (for example, CDT1 in NGC 1232, Castellanos et al. 2002a or S5 in M101, Kinkel & Rosa 1994). For them, an empirical relation between [O III] and [S III] electron temperatures has been used:

$$t([\mathrm{O\,III}]) = 0.95t([\mathrm{S\,III}]) + 0.08$$

based on the grids of photoionization models described in the next section and, differing slightly from the empirical relation found by Garnett (1992), due mainly to the introduction of the new atomic coefficients for S^{2+} from Tayal & Gupta (1999).

Regarding [O II] temperatures, for 81 objects of the sample it has been possible to derive its value from the [O II] (λ3726 + λ3729)/λ7325 line ratio.[1] For the rest of the objects in the sample we have resorted to the model relations between t([O II]) and t([O III]) found in PMD03 that take explicitly into account the dependence of t([O II]) on electron density. This can affect the deduced abundances of O^+/H^+ by non-negligible factors, larger in all cases than the reported errors.

Fig. 1, shows a comparison of the total oxygen abundances derived as described above with the values published in the original sources. The deviations from the one-to-one relation arise mostly in the high-metallicity range as a result of the dependence of t([O II]) on density which affects the calculated O^+/H^+ abundances. This can be better seen in Fig. 2 where the abundance differences are plotted as a function of the O^+/O^{2+} ionic fraction.

The oxygen abundances of the sample objects cover the range 0.02 $Z_\odot$ (IZw18; Skillman & Kennicutt 1993) to 1.82 $Z_\odot$ (CDT1 in NGC 1232; Castellanos et al. 2002a).[2] The re-calculated [S II] electron densities, [O II] and [O III] electron temperatures and oxygen abundances are listed in Table 2. The quoted uncertainties have been derived from the emission-line flux errors as published in the corresponding references. In the upper panel of Fig. 1, the values of these errors (half-error bars) are plotted as a function of oxygen abundance. It can be seen that the errors are almost constant, with an average value of approximately ±0.07 dex, up to 12 + log(O/H) ≃ 8.1

[1] The [O II] λ7319+λ7330 lines can have a contribution by direct recombination which increases with temperature. Using the calculated [O III] electron temperatures, we have estimated these contributions to be less than 4 per cent in all cases and therefore we have not corrected for this effect.

[2] A solar value of 12 + log(O/H) =8.69 (Allende-Prieto, Lambert & Asplund 2001) is assumed through this paper.

Table 1. Bibliographic references for the emission-line fluxes of the compiled sample.

Reference[a]	Object type[b]	Número of points
Castellanos et al. (2002a)*	GEHR	5
Dennefeld & Stasiska (1983)*	DHRs	22
Díaz et al. (1987)*	GEHRs in NGC 604	6
Dinerstein & Shields (1986)	GEHRs	2
Edmunds & Pagel (1984)	GEHRs in NGC 7793	3
French (1980)	HIIGs	13
Garnett & Kennicutt (1994)*	GEHR in M101	1
Garnett et al. (2004)*	GEHRs in M51	2
Garnett et al. (1997)*	GEHRs in NGC 2403	11
González-Delgado et al. (1994)*	GEHR in NGC 2363	13
González-Delgado et al. (1995)*	GEHRs in NGC 7714	5
Guseva et al. (2000)	HIIGs	4
Kennicutt et al. (2003)*	GEHRs in M101	19
Kinkel & Rosa (1994)*	S5 in M101	1
Kniazev et al. (2001)	HIIGs	2
Kunth & Sargent (1983)	HIIGs	13
Kwitter & Aller (1981)	GEHRs in M33	5
Izotov, Thuan & Lipovetsky (1994)	HIIGs	10
Izotov, Thuan & Lipovetsky (1997)	HIIGs	27
Izotov & Thuan (1998)	HIIG	18
Lequeux et al. (1979)	HIIG	8
Pagel et al. (1979)	NGC 300,7	1
Pagel et al. (1992)*	HIIGs	10
Pastoriza et al. (1993)*	GEHRs in NGC 3310	5
Peimbert, Peña & Torres-Peimbert (1986)	NGC 2363	1
Popescu & Hopp (2000)	HIIGs	22
Rayo, Peimbert & Torres-Peimbet (1982)	GEHRs in M101	3
Shaver et al. (1983)	DHRs	7
Shields & Searle (1978)*	GEHRs in M101	2
Skillman et al. (2003)	GEHRs in Sculptor	6
Skillman & Kennicutt (1993)*	IZw18	2
Skillman et al. (1994)*	UGC4483	1
Terlevich et al. (1991)	HIIGs	100
Vílchez et al. (1988)*	GEHRs in M33	5
Vílchez & Esteban (1996)*	DHRs	3
Vílchez & Iglesias-Páramo (2003)	GEHRs in Virgo	9

[a]Those references marked with * give fluxes of the emission lines of [S III] in the near-IR.
[b]GEHR denotes giant extragalactic H II regions, H IIG, H II galaxies and DRH, diffuse H II regions.

and thereafter increase with metallicity up to ±0.5 dex at the highest derived abundances.

The complete table will be available in electronic form as supplementary material in the online version of this paper, at CDS (Centre de Données astronomiques de Strasbourg) via anonymous ftp to cdsarc.u-strasbg.fr (130.79.128.5) (http://cdsweb.u-strasbg.fr), or at http://pollux.ft.uam.es/enrique/table1/. Only an sample is given here.

At any rate, it should be recalled that the determination of the gaseous chemical abundances is usually accomplished by combining results from photoionization models and observed emission-line intensity ratios. Even when the electron temperature can be determined with good accuracy, there are several major unsolved problems that severely limit the confidence of present results including: (1) the effect of temperature structure in multiple-zone models (PMD03); (2) the presence of temperature fluctuations across a given nebula (Peimbert 2003); (3) collisional and density effects on ion temperatures (Luridiana, Peimbert & Leitherer 1999); (4) the presence of neutral zones affecting the determination of ionization correction factors (ICFs; Peimbert, Peimbert & Luridiana 2002); (5) the ionization structure which is not adequately reproduced by current models (PMD03); (6) the possible photon leakage that affects the low-ionization lines formed in the outer parts of the ionized regions (Castellanos, Díaz & Tenorio-Tagle 2002b). The first three effects can introduce uncertainties with respect to the derived oxygen abundances of approximately 0.2, 0.3 and 0.4 dex, respectively, depending on excitation. The uncertainties introduced by the latter effects have not yet been quantified.

3 PHOTOIONIZATION MODELS

In order to identify and understand the possible sources of scatter in the different empirical calibrations, we have calculated a set of photoionization models covering the physical conditions of the observed objects. No attempt has been made, however, to perform recalibrations using these models.

The photoionization models have been computed with the most recent version of the photoionization code CLOUDY 96 (Ferland 2002).

Each modelled H II region has been assumed to be spherically symmetric, with the ionized emitting gas taken to be of constant density (10 and 100 particle cm^{-3}), located at a distance that is

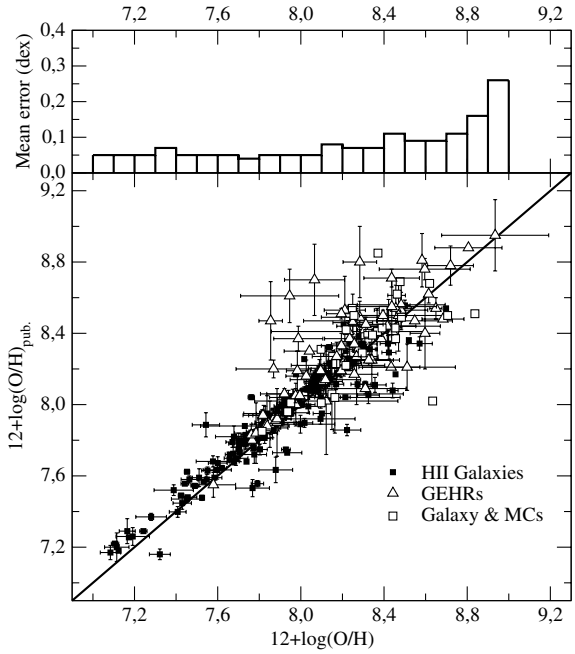

Figure 1. Comparison, for the whole sample, between the oxygen abundances published in the original sources and the abundances as calculated in this work. Symbols for this and subsequent plots are: solid squares for H II galaxies, upward triangles for giant extragalactic H II regions and open squares for diffuse H II regions in the Galaxy and the Magellanic Clouds. The upper panel in the figure shows the distribution of the observational errors (half-error bars) with oxygen abundance.

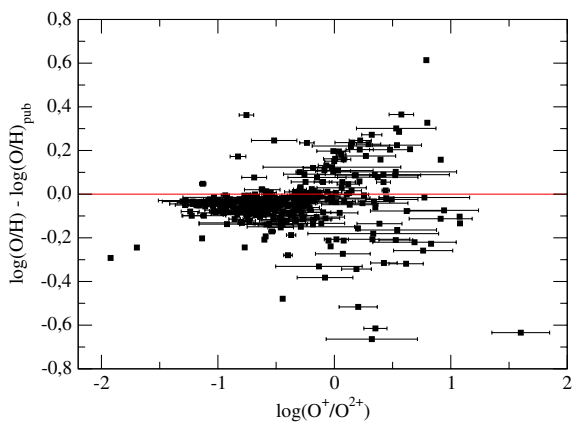

Figure 2. Difference between the oxygen abundances calculated in this work and the published abundances as a function of the (O^+/O^{2+}) ratio. Differences are much larger in the low-excitation regime, where the abundance of O^+ has more weight.

very large compared with its thickness and therefore allowing the approximation of plane-parallel geometry. The gas is ionized by a single massive star, the spectral energy distribution (SED) of which is represented by a CoStar non-local thermal equilibrium (NLTE) stellar atmosphere (Schaerer & de Koter 1997) with an effective temperature of between 35 000 and 50 000 K. The impact on the analysis of the general trends shown by empirical calibrations using other SEDs is negligible and, in practice, only slightly affects the absolute effective temperature scale. Ionization parameters (U) between 10^{-2} and 10^{-3}, which is the range corresponding to the ionization degree shown by the sample objects, have been chosen. Finally, the solar chemical abundances used are those given in Table 3.

We have computed models with values of this solar abundance multiplied by factors of 1.7, 0.85, 0.34, 0.17, 0.08 and 0.04 corresponding to 1, 0.5, 0.2, 0.1, 0.05 and 0.025 times the solar Grevesse & Sauval (1998) value [log(O/H) = −3.08]. The refractory elements: Fe, Mg, Al, Ca, Na and Ni have been depleted by a factor of 10 and Si by a factor of 2 (Garnett et al. 1995), to take into account the presence of dust grains. In the case of nitrogen, we have considered, for the models with $U = 10^{-5/2}$, another set of abundances with a value of (N/O) 0.5 dex lower than the solar value, close to the values found in low-metallicity nebulae.

For the sake of clarity, only the models for $n_e = 100\,\mathrm{cm}^{-3}$, $T_{\mathrm{eff}} =$ 35 000 and 50 000 K, and $U = 10^{-2.0}$ and $10^{-3.0}$ are shown in the figures.

4 EMPIRICAL ABUNDANCE PARAMETERS

4.1 The $R_{23}(O_{23})$ parameter

The R_{23} parameter, that here we have preferred to rename as O_{23} in order to differentiate it from the analogous parameter based on sulphur emission lines, was defined as

$$O_{23} \equiv \frac{I(3727\,\text{Å}) + I(4959\,\text{Å}) + I(5007\,\text{Å})}{I(\text{H}\beta)}$$

by Pagel et al. (1979). Its relation with oxygen abundance for the objects of the compiled sample can be seen in the left-hand panel of Fig. 3. The relation is double-valued. This is due to the efficiency of oxygen as a cooling agent, thus decreasing the strength of the oxygen emission lines at high metallicities. At low metallicities, however, the cooling is mainly exerted by hydrogen and the oxygen line strengths increase with metallicity. The value of log O_{23} reaches a maximum of approximately 1.2 at an oxygen abundance of 12 + log(O/H) ≈ 8.0.

Three different regions can be distinguished in the plot: a lower branch in which O_{23} increases with increasing abundance, an upper branch in which the opposite occurs and a turnover region. The two branches can, in principle, be fitted by regression lines with positive and negative slope, respectively, providing a low to moderate uncertainty in the determination of the metallicity. In the turnover region with $\log O_{23} \geqslant 0.8$ and 12 + log(O/H) ⩾ 8.0, although the precise values are difficult to assess, objects showing the same value of O_{23} can have oxygen abundances that differ by almost an order of magnitude. It should be noted that a large proportion of the data lie on top of this ill-defined zone (up to 40 per cent of the total number of objects and even more in the case of H II galaxies) where the abundance determination can be very uncertain.

Another characteristic of the calibration which is readily apparent is the existence of a scatter larger than accounted for by observational errors. This scatter is related to the fact that, in general, ionized regions do not constitute a single-parameter family, hence different geometries of the emitting gas (ionization parameter) and different ionizing radiation temperatures can affect the values of the abundance parameter O_{23}. This can be seen in the right-hand panel of Fig. 3, where data are shown together with different model sequences. Error bars have been omitted for the sake of clarity. O_{23} is seen to depend on both the ionization parameter and the stellar effective temperature. The dependence on the ionization parameter is more evident at low metallicities, while the dependence on effective temperature is important in all metallicity regimes. This double

Table 2. The calculated electron densities of [S II], electron temperatures of [O II] and [O III] and ionic abundances of O^+ and O^{2+} for some of the whole sample. The results for the whole sample are provided as supplementary online material.

Object	Region	Ref.	n([S II])	t([O III])	$12 + \log(O^{2+}/H^+)$	t([O II])	$12 + \log(O^+/H^+)$	log(O/H)
NGC 628	H13	CDT02	64 ± 42	1.00 ± 0.04	7.70 ± 0.03	–	8.04 ± 0.10	8.20 ± 0.08
NGC 1232	CDT1	CDT02	121 ± 35	0.54 ± 0.09	8.09 ± 0.11	–	8.86 ± 0.27	8.93 ± 0.25
	CDT2	CDT02	20:	1.15 ± 0.19	7.45 ± 0.10	–	7.77 ± 0.28	7.94 ± 0.23
	CDT3	CDT02	198 ± 61	0.82 ± 0.08	7.76 ± 0.07	–	8.38 ± 0.23	8.48 ± 0.21
	CDT4	CDT02	224:	0.93 ± 0.06	7.69 ± 0.04	–	8.08 ± 0.14	8.23 ± 0.12

Table 3. Adopted solar abundances with and without depletion factors for the refractory elements.

Element	Photosphere[a]	Depleted[a]
He[b]	−1.07	−1.07
O[d]	−3.31	−3.31
N[c]	−4.07	−4.07
S[b]	−4.67	−4.67
C[c]	−3.41	−3.41
Ne[b]	−3.92	−3.92
Ar[b]	−5.60	−5.60
Si[c]	−4.47	−4.77
Fe[c]	−4.55	−5.55
Mg[b]	−4.47	−5.47
Al[b]	−5.53	−6.53
Ca[b]	−5.64	−6.64
Na[b]	−5.67	−6.67
Ni[b]	−5.75	−6.75

[a]In terms of $\log(X/H)$. [b]Grevesse & Sauval 1998. [c]Holweger 2001. [d]Allende-Prieto et al. 2001.

dependence makes O_{23} a rather unsuitable abundance parameter. In fact, at an oxygen abundance of $12 + \log(O/H) = 7.8$, log O_{23} can vary between 0.5 and 0.9.

Different assumptions concerning the effects of metallicity on either nebular structure or ionizing temperature have been used by different authors in order to define a sequence of models that would eventually allow the calibration of the upper branch where observational data are very scarce. From analyses of H II region data, McCall, Rybski & Shields (1985) concluded that the stellar ionizing temperature varied with metallicity while the filling factor remained constant, whereas Dopita & Evans (1986) concluded the opposite: that the ionizing temperature was constant while U varied with oxygen abundance. These two different assumptions led to calibrations yielding abundances that differ by more than a factor of 2.

Theoretical stellar evolution models point to a relation between stellar metallicity and effective temperature in the sense that, for a given mass, stars of higher metallicities show lower effective temperatures. This fact led McGaugh (1991, hereafter McG91) to produce a new calibration based on more realistic theoretical models in which the ionization is provided by stellar clusters of different metallicities. According to his models, in the upper branch, O_{23} is relatively insensitive to both the ionizing temperature and U, and the models converge to a single sequence. In the lower branch, however, O_{23} is mostly dependent on U, as has already been shown by Skillman (1989, hereafter S89) and additional information concerning this parameter is needed in order to apply the empirical method with greater confidence.

Some authors have used the [O II]/[O III] ratio as an ionization parameter indicator to obtain this additional information (e.g. Kobulnicky, Kennicutt & Pizagno 1999). The hardness of the ionizing radiation, however, also affects this ratio in a significant way. In fact, at a given value of U, the [O II]/[O III] ratio is lower for higher stellar effective temperatures as a result of increasing the ionization of O^+ to O^{2+}. These effects can be seen in Fig. 4 where log O_{23} is plotted as a function of log ([O II]/[O III]) (left-hand panel) where it can be seen that the [O II]/[O III] ratios corresponding to models with the same ionization parameter and different stellar ionizing temperature differ widely.

Just the opposite happens in the case of [S II]/[S III], another line ratio used as an ionization parameter indicator (e.g. Díaz et al. 1991). At constant U, [S II]/[S III] increases somewhat with increasing stellar effective temperature as more S^{2+} is converted to S^{3+}, although in this latter case the effect is important only for the highest ionization parameters ($U \geqslant 10^{-2}$), thus making the [S II]/[S III] ratio a more useful ionization parameter diagnostic. Fig. 4 (right-hand panel) shows that [S II]/[S III] depends mostly on the ionization parameter and is rather insensitive to the stellar effective temperature.

Regarding observational data, no clear relation is found between log O_{23} and log ([S II]/[S III]), implying that oxygen abundance and the ionization parameter are not correlated. On the other hand, a definite trend between log O_{23} and [O II]/[O III] is clearly seen which can be explained by the expected dependence on stellar effective temperature and metallicity (see also Kewley & Dopita 2002).

Finally, in the turnover region, O_{23} is sensitive to both the ionization parameter and the ionizing temperature, and is almost insensitive to the oxygen abundance.

It should be taken into account that McGaugh models use zero-age star clusters. The situation becomes much more complicated when the evolution of these clusters is taken into account; the evolution of massive stars is fast and metallicity dependent and the cluster ionizing temperature may not be a monotonically decreasing function of age once Wolf–Rayet (WR) stars begin to appear (García Vargas, Bressan & Díaz 1995; Stasińska & Leitherer 1996).

Figs 5 and 6, show the residuals of several published calibrations of the O_{23} parameter in both lower and upper branches as well as in the intermediate region. The calibrations of S89 for the lower branch and Zaritsky, Kennicutt & Huchra (1994, hereinafter ZKH94) for the upper one, involve only the O_{23} parameter. In contrast, the calibrations of McG91 and Pilyugin (2000, 2001a; hereinafter Pil00 and Pil01a, respectively) also take into account the dependence on the ionization parameter and the effective temperature via the ([O II]/[O III]) ratio (Kobulnicky et al. 1999) and the parameter, P, defined as the quotient of [O III] and ([O II]+[O III]) by Pil00.

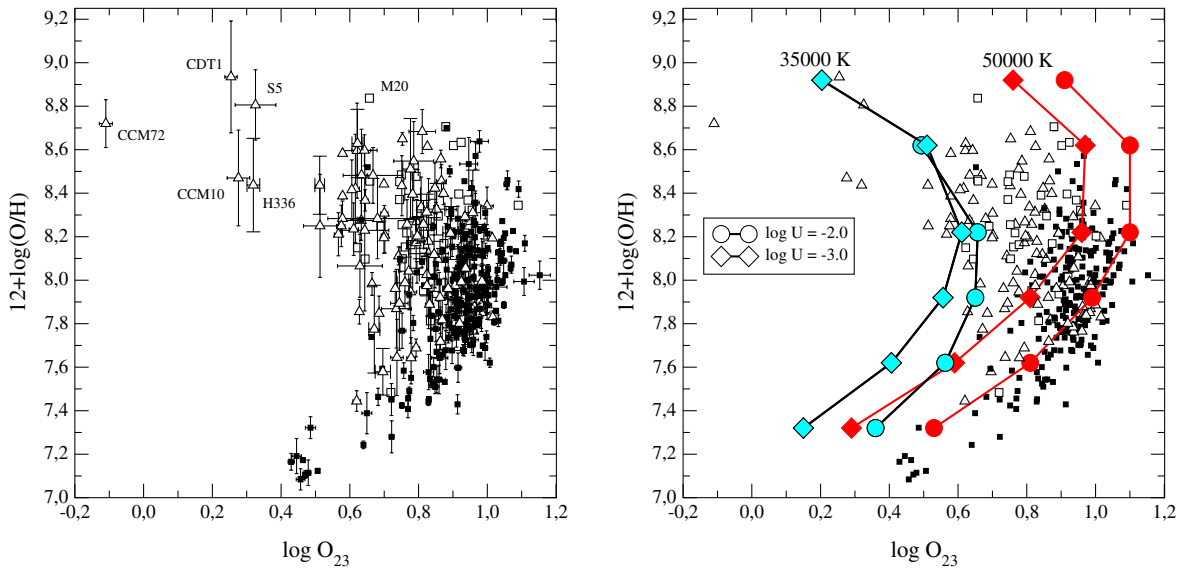

Figure 3. Relation between O_{23} and the metallicity, represented by 12 + log(O/H) (left) and the comparison with CLOUDY photoionization models (right) for different values of the effective temperature (35 000 K, light tone and 50 000 K, dark tone), metallicity (from 0.08 to 1.6 $Z_{\odot}$) and ionization parameter $\log U = -2.0$ (circles) and -3.0 (diamonds).

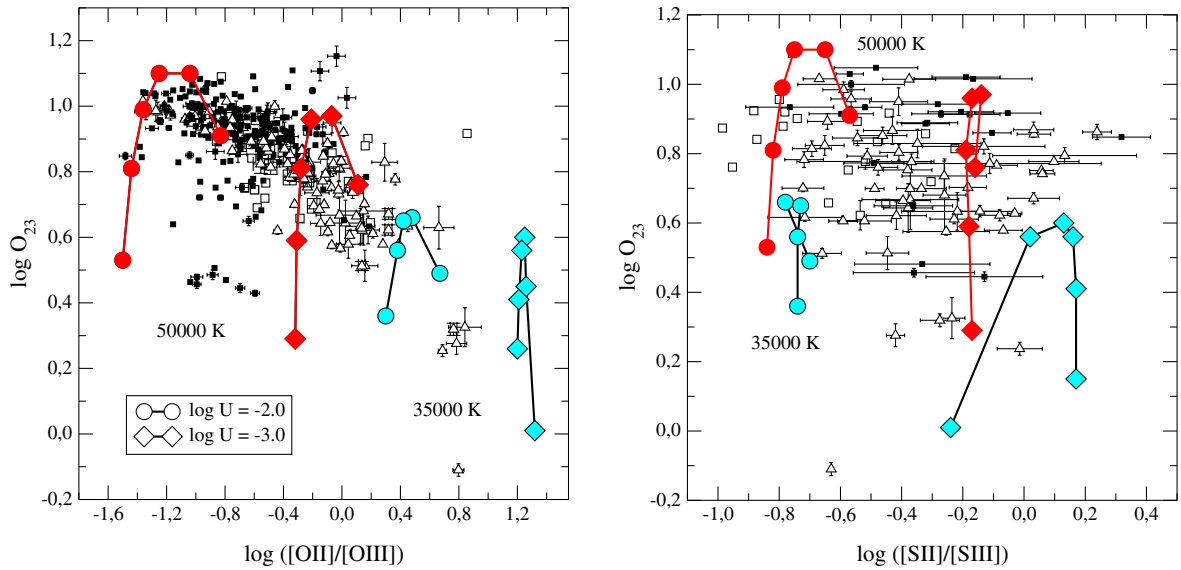

Figure 4. Relation between the O_{23} parameter and the ([O II]/[O III]) ratio, which depends both on the effective temperature and the ionization parameter (left) and the [S II]/[S III] ratio, which depends mostly on the ionization parameter (right). Symbols for the models are the same as in Fig. 3.

For the lower branch, that we have considered as corresponding to 12 + log(O/H) < 8.0, the best fit is found for the calibration by Pil00, with a mean value for the metallicity of 0.03 dex higher than the mean value of those derived directly. Its uncertainty in this regime, understood as the standard deviation of the residuals, is ±0.15 dex which should be compared with the ±0.07 dex average error in the direct oxygen abundance determination (see Fig. 1). The calibrations by Skillman and McGaugh also present the same dispersion, although the mean values of the deduced abundances are 0.06 dex lower and 0.21 dex higher, respectively, than the mean value of those derived directly. A slight trend in the sense of abundances being more underestimated as the metallicity increases is found in the S89 calibration. This trend is probably introduced by the slight dependence of O_{23} on the ionization parameter at high effective temperature that as shown by H II galaxy data in the left-hand panel of Fig. 4.

In fact, in this metallicity range, the O_{23} values predicted by photoionization models for different values of the ionization parameter and the stellar effective temperature produce a scatter in the O_{23} versus 12 + log(O/H) relationship, which is larger than that shown by observational data. This probably indicates that the objects compiled to perform the calibrations, mainly H II galaxies, show very similar properties, i.e. they show a very restricted range of ionization parameters and ionizing temperatures. It should be noted, however, that not all H II galaxies share those properties and that, in particular, those that lack detectable electron temperature sensitive lines and therefore are the probable targets of the empirical calibrations, show ionization parameters which are significantly lower. These include

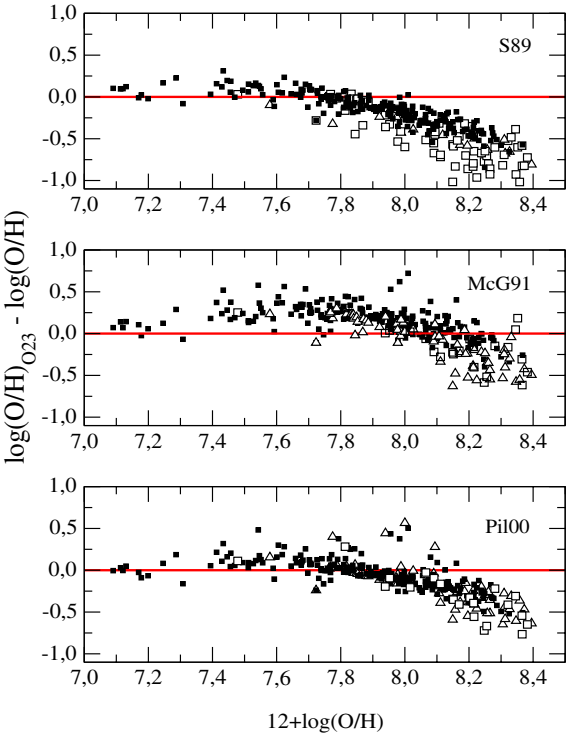

Figure 5. Residuals of the metallicities deduced from the Skillman (1989; upper panel), McGaugh (1991; middle panel) and Pilyugin (2000; lower panel) calibrations as a function of the directly derived abundances for the lower branch of the O_{23} versus O/H plot.

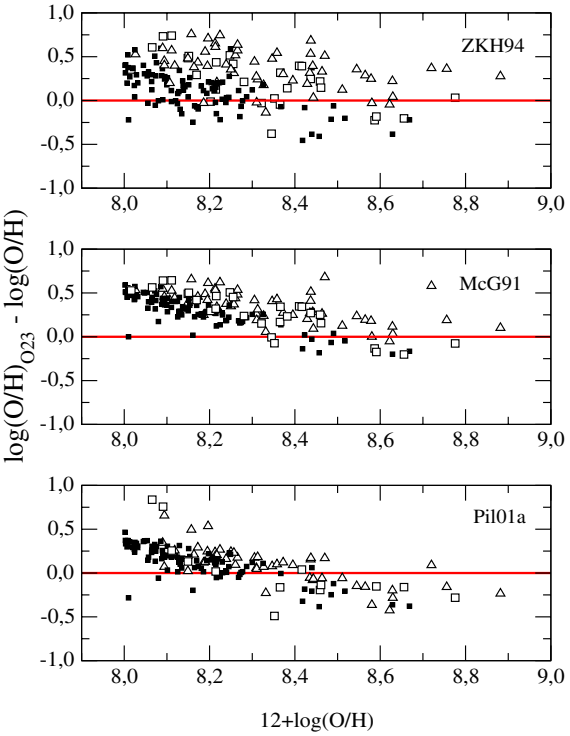

Figure 6. Residuals of the metallicities deduced from the ZKH94 (upper panel), McGaugh (1991; middle panel) and Pilyugin (2001a; lower panel) calibrations as a function of the directly derived abundances for the upper branch of the O_{23} versus O/H plot.

luminous compact blue galaxies (LCBGs; Hoyos & Díaz 2005).

For the upper branch, in the range $12 + \log(\mathrm{O/H}) \geqslant 8.4$ the best fit is found with McG91 calibration, although it predicts abundances 0.08 dex larger than the mean value, with a dispersion of 0.19 dex. Taking into account that the average error in the direct oxygen abundance determination in this regime is approximately ± 0.20, this calibration provides a good estimate of the oxygen abundance for metallic objects. The calibration by Pil01a underestimates abundances by 0.14 dex on average with a dispersion of 0.21 dex. Contrary to what is found for the lower branch, the only calibration not taking into account the dependences on log U and T_{eff} (ZKH94) shows the largest dispersion (0.27 dex) which probably implies that, in this case, the calibrating sample objects do not share ionizing properties.

Finally, for the intermediate region, in the range $8.0 \leqslant 12 + \log(\mathrm{O/H}) < 8.4$, we have evaluated the calibrations for both the lower and upper branches. In this case it can be observed that the lower-branch calibrations underestimate the metallicity and the upper-branch calibrations overestimate it with residuals that increase with increasing and decreasing metallicity, respectively. In this regime it is virtually impossible to choose any reliable calibration of O_{23}.

There are not many ways to improve on the O_{23} abundance parameter calibration, since H II regions and H II galaxies are ionized by young star clusters and, as these clusters evolve, their ionization parameters and ionizing temperatures change in ways that are not easy to parametrize. A more promising approach is the search for other potentially useful abundance parameters, some of which are examined below.

4.2 Parameters involving [N II]

The $N2$ parameter was defined as

$$N2 \equiv \log \frac{I(6584\ \text{Å})}{I(\mathrm{H}\alpha)}$$

by Denicoló, Terlevich & Terlevich (2002, hereinafter DTT02), although it was used before as an empirical estimator by Storchi-Bergmann et al. (1994) and Van Zee et al. (1998). The relation between $N2$ and the logarithmic oxygen abundance is shown in the left-hand panel of Fig. 7 for all the objects in the sample for which nitrogen data exists. The $N2$ parameter has several advantages: first of all, contrary to O_{23}, the relationship between $N2$ and oxygen abundance is single-valued and secondly, since the emission lines on which it is based are very close in wavelength, the $N2$ parameter is almost free of uncertainties introduced by reddening corrections or flux calibrations. The dash-dotted line in the plot corresponds to the relation found by DTT02, for their sample objects:

$$12 + \log(\mathrm{O/H}) = 9.12 + 0.73N2.$$

This line represents a reasonable fit to the data, but shows a large scatter at all metallicities. Most of the scatter is shown by GEHR data, while H II galaxies define a much narrower relation. Most GEHR data fall below the line. This is not surprising since many of the metal-rich GEHR used by DTT02 in their calibration had oxygen abundances derived from O_{23} and directly derived abundances for metal-rich H II regions tend to be lower than those derived from this parameter (Castellanos et al. 2002a; Garnett et al. 2004).

Again, the main reason for the dispersion is probably related to the different ionization parameters and stellar effective temperatures of

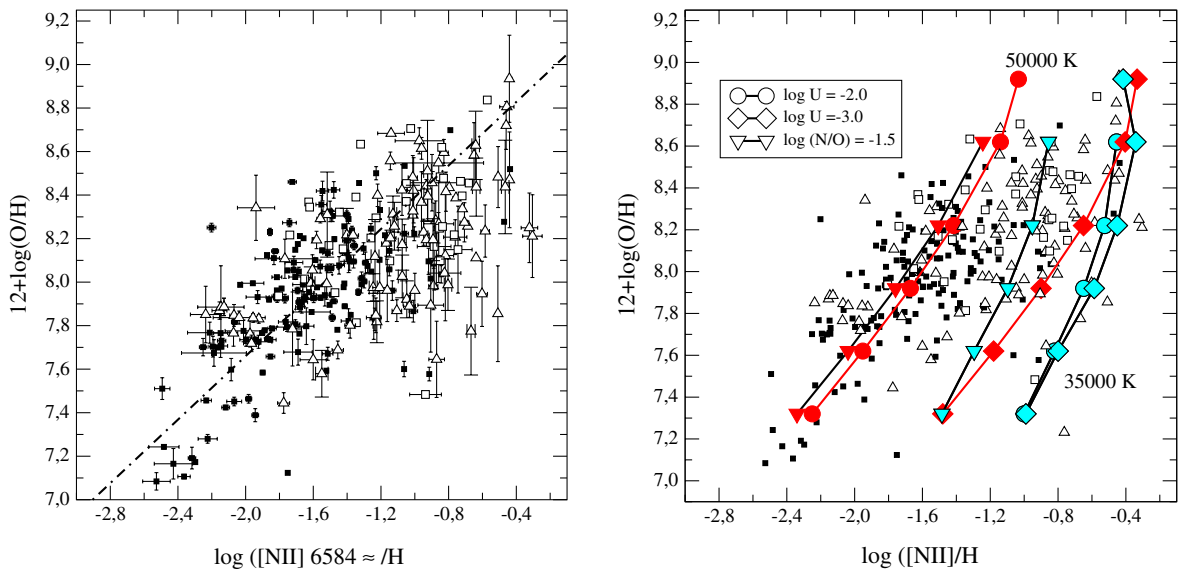

Figure 7. Relation between $N2$ and 12 + log(O/H) (left) and the comparison with CLOUDY photoionization models (right) for different values of effective temperature (35 000 K, light tone and 50 000 K, dark tone), metallicity (from 0.08 to 1.6 $Z_{\odot}$) and ionization parameter log $U = -2.0$ (circles) and -3.0 (diamonds).

GEHR since the $N2$ parameter depends on both as can be seen in the right-hand panel of Fig. 7. The [N II] lines become weaker as the excitation degree and/or the ionizing temperature increase. $N2$ reaches a maximum of approximately -0.5 for models with low effective temperature (35 000 K), while the lowest values of the parameter are found in models with high effective temperature (50 000 K) and high ionization parameter ($\log U = -2.0$). An additional source of scatter is related to the possibly different N/O relative abundances. To try to quantify this effect we have added a set of photoionization models with a value of log (N/O) 0.5 dex lower than our assumed solar value (see Table 3) and log $U = 10^{-5/2}$. This model sequence can also be seen in Fig. 7 (right-hand panel). A lower N/O ratio mimics a higher ionization parameter. Model sequences of high ionizing temperatures and constant N/O ratio seem to reproduce H II galaxy data adequately, while a sequence of models with N/O increasing with oxygen abundance would seem more adequate for GEHR data.

The residuals of the fit from the DTT02 calibration against the directly determined oxygen abundances are represented in Fig. 8. This empirical calibrator works reasonably well in the turnover region of the log O_{23} versus 12 + log(O/H) plot, although the dispersion reaches a value of 0.27 dex for the reasons given above. This dispersion is of 0.25 dex for H II galaxies. For the rest of the sample it reaches 0.3 dex with the mean value being 0.1 dex higher, thus implying that, in these cases, oxygen abundances could be overestimated.

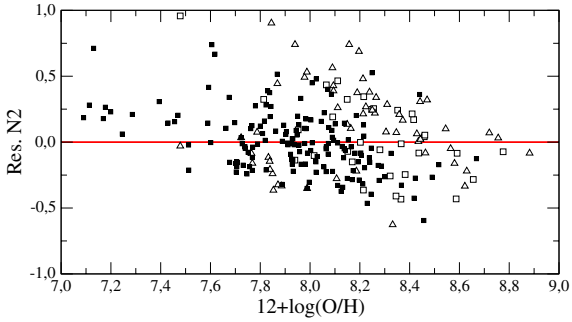

Figure 8. The residuals of the fit by the Denicoló et al. (2002) calibration and the directly derived abundances as a function of the oxygen abundance for the compiled data.

Other empirical parameters involving the [N II] lines are the [N II] λλ6548,6584/[O III] λλ4959,5007 ratio, first proposed by Alloin et al. (1979) and recently revindicated by Pettini & Pagel (2004), and the [N II] λλ6548,6584/[O II] λλ3727,3729 and [N II] λλ6548,6584/[S II] λλ6716,6731 ratios suggested by Dopita & Evans (1986) and Kewley & Dopita (2002) as metallicity calibrators in the high-abundance regime. In Fig. 9, 12 + log(O/H) is represented as a function of the [N II]/[O III] parameter (top panel), the [N II]/[O II] parameter (middle panel) and the [N II]/[S II] parameter (bottom panel) for the compiled sample of objects. From the direct comparison with observational data, it can be seen that these three parameters are valid only for a metallicity higher than 12 + log(O/H) ≈ 7.8 and with a scatter similar to that found for the $N2$ parameter. This scatter could again be related to the different objects presenting different N/O ratios. In fact, a clear segregation is found between H II galaxy and GEHR data, more evident in the upper panel, which is probably related to the GEHR showing higher values of N/O and hence N/S ratios. Fig. 10 (upper panel) shows that a tight relation exists between log ([N II]/[O II]) and log (N^+/O^+) that is, in turn, a very good indicator of log(N/O). The fit of a regression line to the data produces the relation

$$\log\left(\frac{\mathrm{N}}{\mathrm{O}}\right) = 1.144 \log\left(\frac{[\mathrm{N\,II}]}{[\mathrm{O\,II}]}\right) - 0.232.$$

The uncertainty involved in the determination of the N/O ratio from [N II]/[O II] for the whole sample, represented by the standard deviation of the residuals, is 0.14 dex, but decreases to only 0.08 for H II galaxies (see Fig. 10, lower panel).

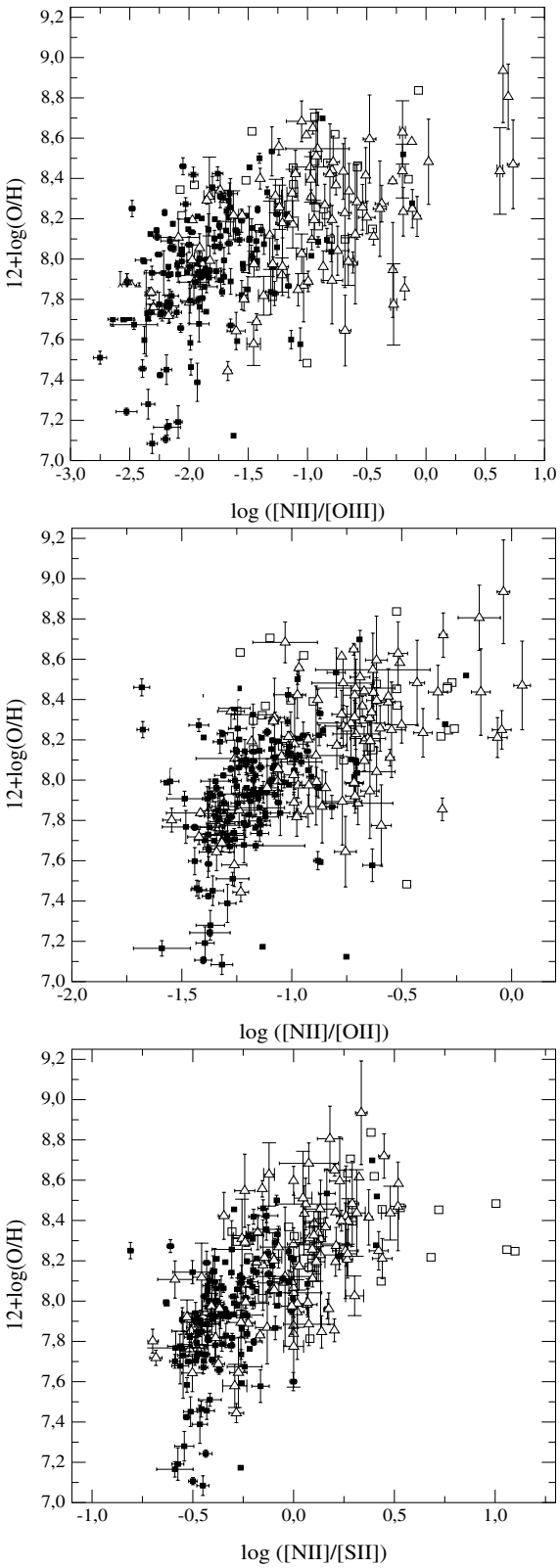

Figure 9. Relation between the [N II]/[O III] (top panel), [N II]/[O II] (middle panel) and [N II]/[S II] (bottom panel) ratios and the metallicity, represented by 12 + log(O/H).

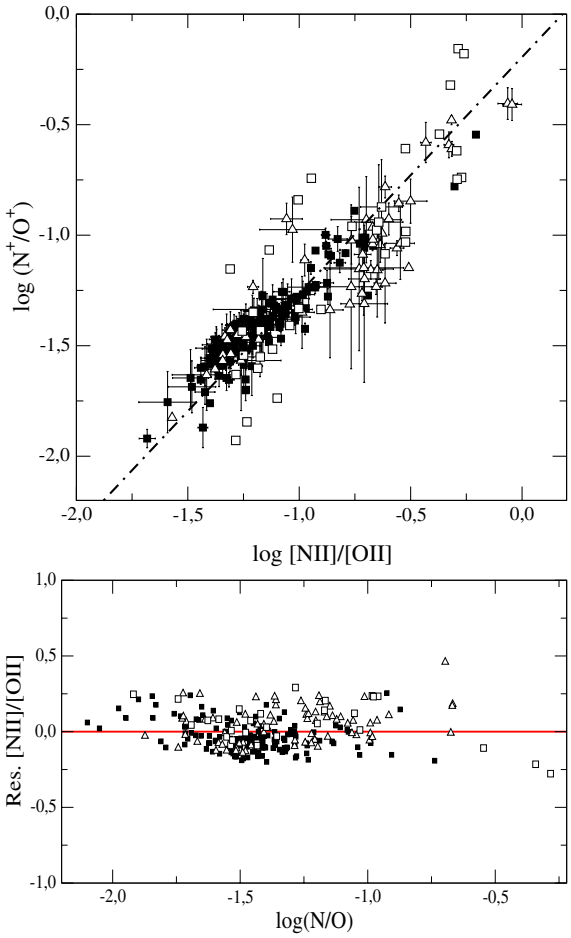

Figure 10. Upper panel: relation between the [N II]/[O II] ratio and the (N^+/O^+) value for the objects of the sample. The dotted-dashed line shows the empirical calibration deduced. Lower panel: the residuals of the fit as a function of the N/O ratio.

4.3 The $S_{23(4)}$ parameter

The S_{23} parameter was defined by Vílchez & Esteban (1996) as

$$S_{23} \equiv \frac{I(6717\,\text{Å}) + I(6731\,\text{Å}) + I(9069\,\text{Å}) + I(9532\,\text{Å})}{I(\text{H}\beta)}$$

using the [S II] and [S III] lines analogous to those of [O II] and [O III] in the O_{23} parameter. It was proposed by Christensen, Petersen & Gammelgaard (1997) as a sulphur abundance indicator and more recently by DPM00 as an oxygen abundance indicator due to the characteristics evident in Fig. 11 (left-hand panel) first, its single-valued behaviour up to solar metallicities, and secondly its lower dependence on the other functional parameters. The fact that S_{23} presents a lesser dependence on the effective temperature and the ionization parameter than O_{23}, seems to be confirmed by photoionization models (see Fig. 11, right-hand panel). There is a dependence of S_{23} on log U and T_{eff} but it is weaker than for O_{23} (see Fig. 3 for a comparison).

From the observational point of view, the S_{23} parameter has two important advantages: first, the sulphur lines remain intense even for the highest metallicity objects and, secondly, it is relatively independent of reddening, since the lines of both [S II] and [S III] can be measured relative to nearby hydrogen recombination lines. On

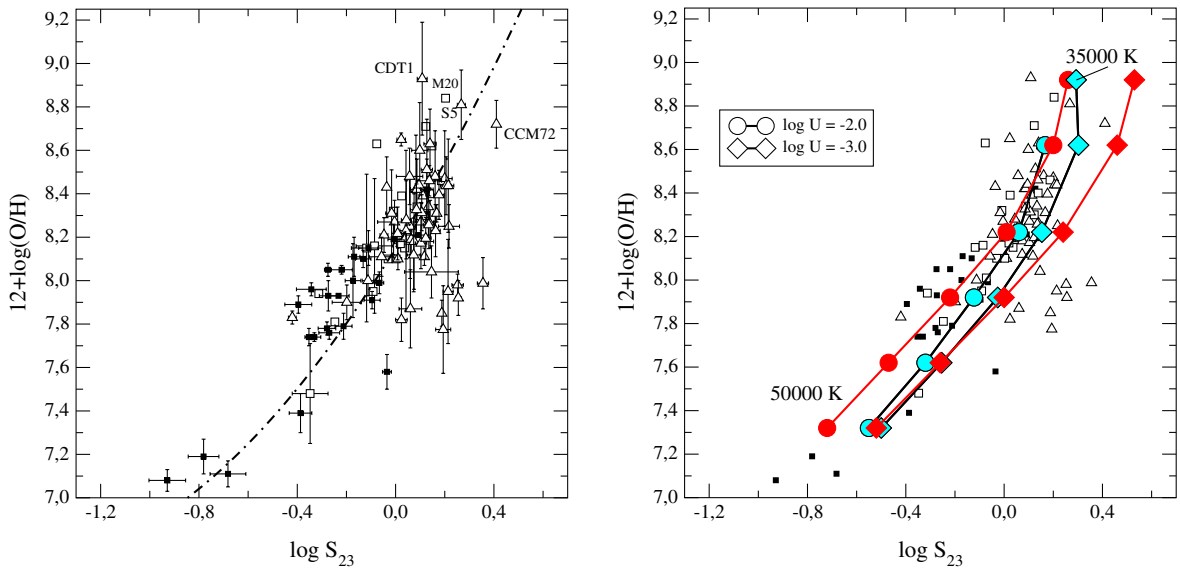

Figure 11. Relation between log S_{23} and the metallicity, represented by $12 + \log(\mathrm{O/H})$ (left) and the comparison with CLOUDY photoionization models (right) for different values of the effective temperature (35 000 K, light tone and 50 000 K, dark tone), metallicity (from 0.08 to 1.6 $Z_{\odot}$) and ionization parameter $\log U = -2.0$ (circles) and -3.0 (diamonds). The dashed-dotted line shows the calibration derived in this work.

the negative side, [S III] lines shift out of the far-red spectral region for redshifts higher than 0.1.

Using the newly added observational data we have improved the DPM00 relation to

$$12 + \log(\mathrm{O/H}) = 8.15 + 1.85 \log S_{23} + 0.58(\log S_{23})^2$$

the residuals of which for the complete sample relative to the directly determined oxygen abundances are represented as a function of oxygen abundance in the upper panel of Fig. 16 (see Section 4.4). The dispersion is approximately equal to 0.2 dex in all the abundance ranges, although it decreases to 0.10 dex for the H II galaxy sample. The relation is not linear. Values of S_{23} lower than expected are found for higher excitation nebulae having low metallicity, probably due to the presence of [S IV] in non-negligible amounts, as seems to be indicated by the position on the diagram of IZw18 (the least metallic object). Unfortunately, despite recent observations of a sample of H II galaxies in the near-IR spectral range (PMD03), there is a considerable lack of data on objects of low metallicity where the inclusion would definitely improve the calibration.

Oey & Shields (2000) have defined a new parameter, S_{234},

$$S_{234} \equiv \frac{I(6725\,\text{Å}) + I(9069\,\text{Å}) + I(9532\,\text{Å}) + I(10.5\,\mu\text{m})}{I(\text{H}\beta)}$$

which takes into account the contribution of [S IV] through its emission line at 10.52 μm. The contribution of [S IV] is expected to be relevant only in objects with a high degree of ionization (Díaz et al. 1991) and therefore the use of S_{234} almost eliminates the dependence on the ionization parameter found for S_{23} (Kennicutt et al. 2000). In fact, photoionization models indicate that S_{23} is only slightly dependent on the ionization parameter but shows a non-negligible dependence on the effective temperature, which becomes more evident at high metallicities (see Fig. 12).

Unfortunately, the sample of objects for which the [S IV] line in the mid-infrared is measured is very poor. Using the available data for these objects we have confirmed that the contribution of this line to S_{234} can be rather large. We have found very little [S IV] data for H II regions, GEHR and H II galaxies: the Orion nebula (Lester, Dinerstein & Rank 1979), Mrk 209 (Nollenberg et al. 2002) and a sample of objects in the Magellanic Clouds (Vermeij et al. 2002). Data on these objects are plotted in Fig. 13 (S_{23} in the left-hand panel and S_{234} in the right-hand panel). Any improvement in the abundance calibration is difficult to quantify given the scarcity of data. At any rate, since no observations of the 10.5-μm line exist for most objects, it would have to be calculated from photoionization models which would make S_{234} a semi-empirical parameter.

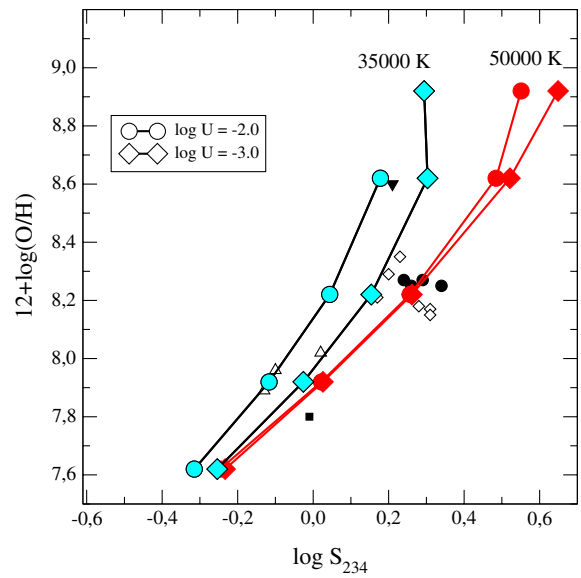

Figure 12. Comparison between observations and model results for the relation between the S_{234} parameter and the oxygen abundance.

4.4 The S_{23}/O_{23} parameter

One fact that becomes evident from the examination of the different abundance parameters discussed above is that the validity of each one of them seems to be restricted to a given metallicity range.

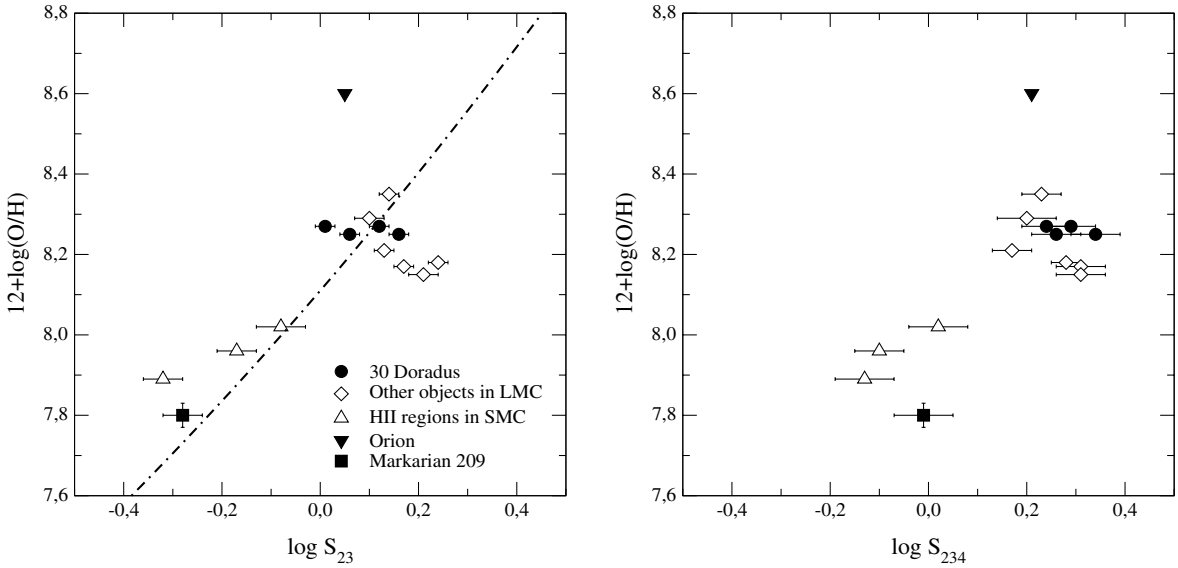

Figure 13. Relation between log S_{23} (left) and log S_{234} (right) and the oxygen abundance for the sample of objects with a direct measurement of the [S IV] 10.52-μm line: Mrk 209 (filled square), Orion (filled triangle), 30 Doradus (filled circles) and objects from the Large Magellanic Cloud (LMC) (open diamonds) and the Small Magellanic Cloud (SMC) (open triangles).

This means that it is necessary to have some a priori knowledge concerning the metallicity of an object or a sample of objects in order to choose the appropriate abundance indicator.

Traditional ways of doing this include an examination of the [N II] λ6584/Hα ratio that can discriminate between objects with 12 + log(O/H) higher or lower than approximately 8.0 (S89). More recently, the values of the O_{23} and S_{23} taken together have been used by DPM00 to discriminate between subsolar and oversolar abundances. However, in some cases, interest has focused on the comparison of global abundance trends shown by different objects or abundance distributions over a wide range of metallicities. In those cases it would be desirable to obtain abundances by means of the same calibrator so that comparisons are meaningful. This calibrator should be valid for the whole metallicity range.

The study of metallicity gradients over galaxy discs is one of the issues that could be improved in this way. For example, there are many different conclusions concerning the value of the oxygen abundance distribution in the well-studied galaxy M101. Different authors (Scowen, Dufour & Hester 1992; Vila-Costas & Edmunds 1992; Zaritsky 1992) have pointed to an increase in the slope of the gradient in the inner regions, whereas other authors (Henry & Howard 1995; Pilyugin 2001b) obtain an exponential law throughout the whole disc. Kennicutt & Garnett (1996) have shown how the use of one calibration of O_{23} or another leads to different conclusions.

In Fig. 14 we represent the gradient of some of the parameters studied here as a function of the galactocentric distance to the centre of M101 (data from Kennicutt & Garnett 1996). In the upper panel the O_{23} parameter is seen to increase with increasing galactocentric radius up to a value of $0.3R_0$ and then it remains almost constant. In the middle panel, the S_{23} parameter shows the same behaviour as O_{23} in the central regions of the disc but decreases with increasing galactocentric radius from $0.3R_0$ onwards. These two trends taken together point to the central disc regions of M101 ($R < 0.3R_0$) being oversolar and thus lying on the upper branch of the O_{23} and S_{23} parameters. The outer regions of the disc would have undersolar abundances and lie on the lower branch of the S_{23} calibration. Most of the regions in this regime ($R > 0.3R_0$) lie on the turnover

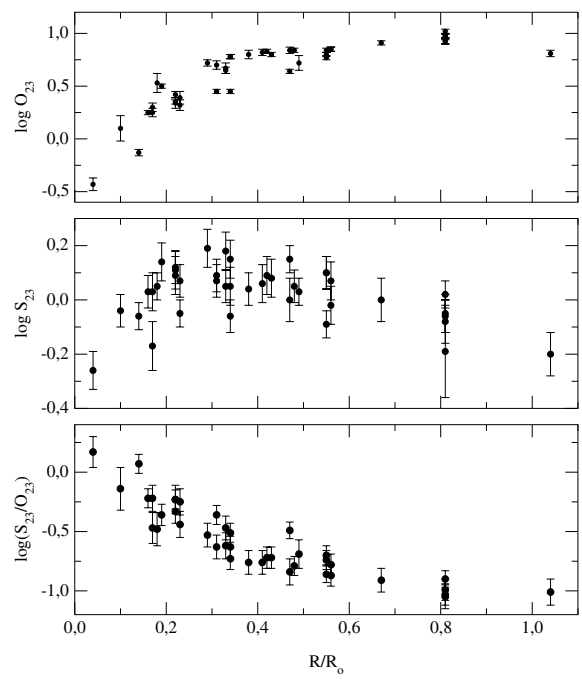

Figure 14. Variation of log O_{23} (top panel), log S_{23} (middle panel) and log(S_{23}/O_{23}) (bottom panel) with normalized galactocentric distance for M101 (data from Kennicutt & Garnett 1996).

region of the O_{23} calibration and therefore show an almost constant value of this parameter. In the lower panel of Fig. 14, we can see that a combination of the two parameters, S_{23}/O_{23}, shows a continuously decreasing trend through the disc of M101.

Using all the objects of our sample with measurements of the [O II], [O III], [S II] and [S III] lines and a direct determination of the metallicity, we have calibrated this new parameter for the first time (Fig. 15 left-hand panel). As can be seen, the relation remains single-valued for the whole range of metallicity, though it is non-linear, due probably to the contribution of [S IV] for high-excitation

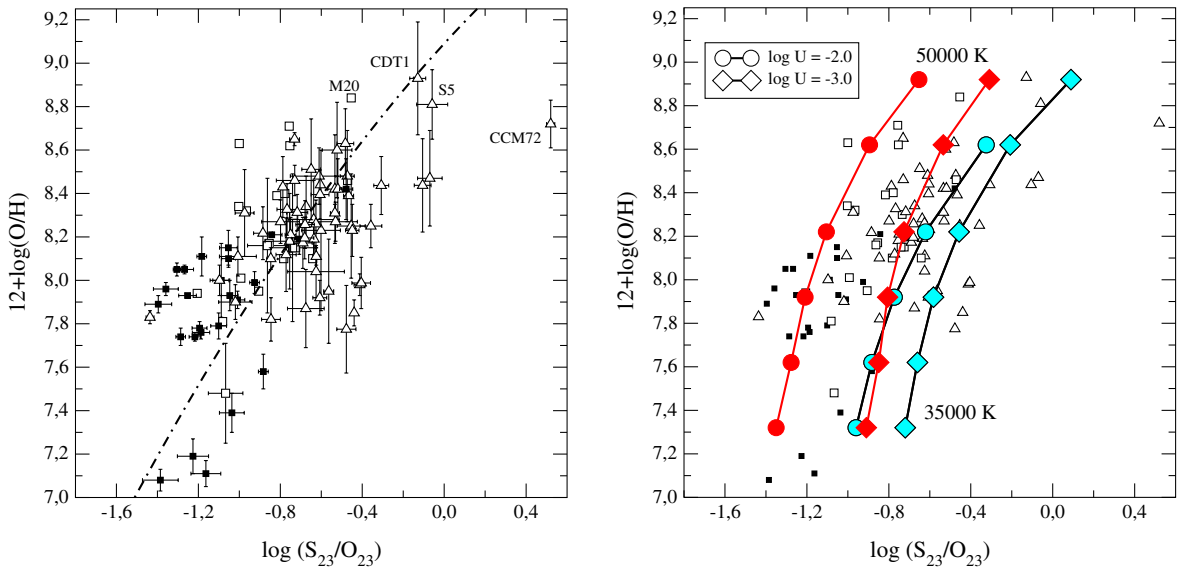

Figure 15. Relation between $\log(S_{23}/O_{23})$ and the metallicity, represented by $12 + \log(\mathrm{O/H})$ (left) and the comparison with CLOUDY photoionization models (right) for different values of effective temperature (35 000 K, light tone and 50 000 K, dark tone), metallicity (from 0.08 to 1.6 $Z_{\odot}$) and ionization parameter $\log U = -2.0$ (circles) and -3.0 (diamonds). The dashed-dotted line corresponds to the calibration proposed in this work.

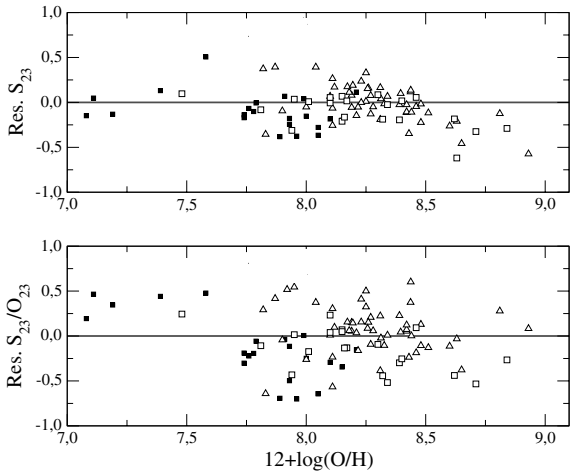

Figure 16. Residuals of the abundances determined from the calibration with S_{23} (upper panel) and S_{23}/O_{23} (bottom panel) to those derived directly, as a function of abundance.

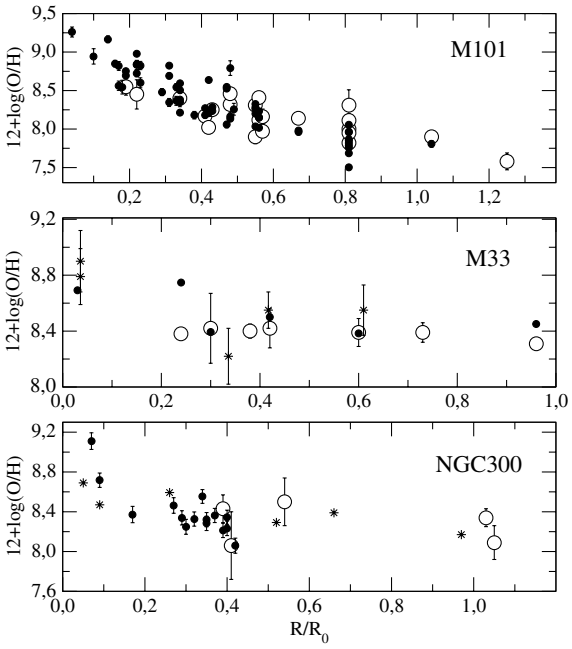

Figure 17. Metallicity gradients of M101, M33 and NGC 300. Filled circles: abundances derived from the S_{23}/O_{23} parameter; open circles: abundances derived from the direct method; asterisks: abundances derived for early-type stars (see the text for details).

regions of low metallicity. The addition of high-metallicity objects is not possible due to the lack of data with the necessary auroral lines, but the fact that the parameter increases towards the inner parts of the disc of M101 (see Fig. 14) suggests that it does not undergo any turnover at high metallicities. Of course, this parameter keeps the same sources of uncertainty as its two progenitors. In Fig. 15 (right), where we compare the observational data with results from our photoionization models, it can be seen that the value of S_{23}/O_{23} increases for low degrees of ionization and lower effective temperatures.

Using the compiled data, we propose the following relation to derive oxygen abundances in the whole metallicity range in the absence of auroral emission-line data:

$$12 + \log(\mathrm{O/H}) = 9.09 + 1.03 \log\left(\frac{S_{23}}{O_{23}}\right) - 0.23 \left[\log\left(\frac{S_{23}}{O_{23}}\right)\right]^2.$$

This relation is plotted along with data in the left-hand panel of Fig. 15. The residuals of this fit from the values of $12 + \log(\mathrm{O/H})$ deduced from the direct method, are plotted in the lower panel of Fig. 16 and show a dispersion of 0.27 dex, comparable to that found for the $N2$ parameter.

The upper panel of Fig. 17 shows the oxygen abundance gradient in M101. Solid circles correspond to oxygen abundances derived using the S_{23}/O_{23} parameter from the emission-line data of Kennicutt & Garnett (1996); open circles correspond to abundances derived

by the direct method (Kennicutt et al. 2003). The agreement between directly determined and empirically derived abundances is excellent.

Unfortunately, sulphur line intensity data are scarce and therefore it is difficult to assess the suitability of the S_{23}/O_{23} parameter as an abundance gradient indicator. We have found only two more galaxies with data covering a substantial part of the disc: M33 (data from Kwitter & Aller 1981; Vílchez et al. 1988) and NGC 300 (data from Deharveng et al. 1988; Christensen et al. 1997). Their abundance gradients are shown in the middle and lower panels of Fig. 17, respectively. Again, solid circles correspond to oxygen abundances derived using the S_{23}/O_{23} parameter and open circles correspond to abundances derived by the direct method. We have also added oxygen abundance data derived from the spectroscopic analysis of early B-type supergiant stars (Monteverde et al. 2000; Urbaneja et al. 2003). Although the discs of these two galaxies are not as well sampled as that of M101, the agreement between empirically and directly derived abundances is good and the agreement between nebular and stellar abundances is encouraging. Regarding the shape of the gradients, in all three cases an increase in slope for the central galactic regions is apparent, although in the cases of M33 and NGC 300 nothing conclusive can be said. We think that more observations and more work along these lines would greatly help to derive the true abundance distributions across the discs of galaxies.

5 SUMMARY AND CONCLUSIONS

In this work we have revised the different proposed oxygen abundance calibrations using a large compiled sample of observations comprising the emission lines of [O II], [O III], [S II], [S III] and [N II] for objects with oxygen abundances derived by the direct method. The data have been compared with results from a set of photoionization models in order to seek an explanation to the sources of scatter in the calibrations. The direct calibration of any parameter with model results alone would lead to non-quantifiable systematic errors and we consider strictly empirical calibrations to be much more reliable.

In Table 4 we summarize the main properties of the parameters studied, including their metallicity range of validity, and the uncertainty obtained for each calibration, understood as the standard deviation of the residuals of the deduced oxygen abundance and that derived through the direct method. The O_{23} parameter is the most widely used, due to the important role of oxygen in the cooling of the ionized gas and because the oxygen emission lines remain in the optical–far-red part of the spectrum until a redshift of $\approx$1. This parameter presents a double-valued relation with metallicity and in the lower and upper branch (in the latter case, taking into account the strong dependence on effective temperature) the uncertainty remains below 0.2 dex. Nevertheless, the uncertainty in the turnover region [for 12 + log(O/H) between 8.0 and 8.4] may reach almost an order of magnitude. No methods of improving this calibration further have been found in this work.

Table 4. Summary of the properties of the different empirical calibrators. The uncertainty is found from the standard deviation of the residuals of each parameter with the oxygen abundance derived directly. See the text for the mean deviations.

Parameter	Range of Z^a	Uncertainty^b
O_{23} (lower branch)	$Z < 8.0$	0.13 (Pil00, McG91)
O_{23} (int. region)	$8.0 \leqslant Z < 8.4$	≈ 0.70
O_{23} (upper branch)	$Z \geqslant 8.4$	0.19 (McG91)
$N2$	All Z (H II galaxies)	0.25
S_{23}	Until 8.9	0.20
S_{23}/O_{23}	All Z	0.27

^{a} Z represents 12 + log(O/H). ^{b}In logarithmic units, dex.

The best alternative to this parameter in this metallicity regime is S_{23}. In objects where it is possible to observe the near-IR [S III] lines (up to a redshift of $\approx$0.1), the metallicity can be deduced with less than 0.2 dex dispersion up to oxygen abundances of 12 + log(O/H) $\approx$ 8.9. The S_{23} parameter also offers the advantage of being relatively independent of reddening. The contribution of the [S IV] emission line in the mid-IR is relevant only for high-excitation objects and can be taken into account by means of the S_{234} parameter. Unfortunately, there is, at the moment, very little data to calibrate it empirically, and available photoionization models fail to correctly reproduce the ionization structure for sulphur (PMD03).

The $N2$ parameter, which is also reddening independent, is a good alternative for distant objects (up to $z \approx 0.5$) with intermediate metallicity [$8.0 \leqslant 12 + \log(\mathrm{O/H}) \leqslant 8.4$]. Nevertheless, this parameter suffers from uncertainties due to its dependence on the ionization parameter and the N/O ratio. Besides, the calibration performed by DTT02 works better for H II galaxies data but its application to higher metallicity regions carries a higher uncertainty and possibly overestimates the derived oxygen abundances.

Regarding the [N II]/[O III], [N II]/[O II] and [N II]/[S II] parameters, these are only correlated with oxygen abundances at moderate to high metallicities and show an uncertainty similar to that of $N2$. However, as the main source of uncertainty for the calibrations involving the nitrogen lines is probably related to the N/O ratio, these calibrations could be improved with the use of [N II]/[O II] as an N/O calibrator which shows a dispersion of only 0.10 dex for H II galaxies.

Finally, we have used the compiled sample of objects to produce for the first time a calibration for the S_{23}/O_{23} parameter, which could be useful for studying variations over a wide range of metallicities, as is the case for the discs of galaxies. This new parameter includes non-negligible uncertainties, inherited from its two predecessors, O_{23} and S_{23} but the results for the disc of M101 are encouraging.

ACKNOWLEDGMENTS

We would like to thank M. Castellanos, R. Terlevich, E. Terlevich, C. Esteban, E. Pérez and D. Valls-Gabaud for very interesting discussions and suggestions and an anonymous referee for a careful revision of the manuscript. We would also like to acknowledge the thorough revision of the English performed by Michael Taylor. This work has been partially supported by DGICYT projects AYA-2000-0973 and AYA-2004-08260-C03-03.

REFERENCES

Allende-Prieto C., Lambert D. L., Asplund M., 2001, ApJ, 556, 63
Alloin D., Collin-Souffrin S. Joly M., Vigroux L., 1979, A&A, 78, 200
Belley J., Roy J.-R., 1992, ApJS, 78, 61
Castellanos M., Díaz A. I., Terlevich E., 2002a, MNRAS, 329, 315 (CDT02)
Castellanos M., Díaz A. I., Tenorio-Tagle G., 2002b, ApJ, 565, L79
Christensen T., Petersen L., Gammelgaard P., 1997, A&A, 322, 41
Deharveng L., Caplan J., Lequeux J., Azzopardi M. Breysacher J., Tarenghi M., Westerlund B., 1988, A&AS, 73, 407
Denicoló G., Terlevich R., Terlevich E., 2002, MNRAS, 330, 69 (DTT02)
Dennefeld M., Stasiska G., 1983, A&A, 118, 234
De Robertis M. M., Dufour R. J., Hunt R. W., 1987, JRASC, 81, 195
Díaz A. I., Pérez-Montero E., 2000, MNRAS, 312, 130 (DPM00)

Díaz A. I., Terlevich E., Pagel B. E. J., Vílchez J. M., Edmunds M. G., 1987, MNRAS, 226, 19
Díaz A. I., Terlevich E., Vílchez J. M., Pagel B. E. J., Edmunds M. G., 1991, MNRAS, 253, 245
Dinerstein H. L., Shields G. A., 1986, ApJ, 311, 45
Dopita M. A., Evans I. N., 1986, ApJ, 307, 431
Edmunds M. G., Pagel B. E. J., 1984, MNRAS, 211, 507
Ferland G. J., 2002, Univ. Kentucky Internal Report, HAZY: a brief introduction to CLOUDY.
French H. B., 1980, ApJ, 240, 41
García Vargas M. L., Díaz A. I., Bressan A., 1995, A&AS, 112, 13
Garnett D. R., 1992, AJ, 103, 1330
Garnett D. R., Kennicutt R. C., 1994, ApJ, 426, 123
Garnett D. R., Dufour R. J., Peimbert M., Torres-Peimbert S., Shields G. A., Skillman E. D., Terlevich E., Terlevich R., 1995, ApJ, 449, 77
Garnett D. R., Shields G. A., Skillman E. D., Sagan S. P., Dufour R. J., 1997, ApJ, 469, 93
Garnett D. R., Kennicutt R. C., Bresolin F., 2004, ApJ, 607, L21
González-Delgado R. M. et al. 1994, ApJ, 437, 239
González-Delgado R. M., Pérez E., Díaz A. I., García-Vargas M. L., Terlevich E., Vílchez J. M., 1995, ApJ, 439, 604
Grevesse N., Sauval A. J., 1998, SSRv, 85, 16
Guseva N. G., Izotov Y. I., Thuan T. X., 2000, ApJ, 531, 776
Henry R. B. C., Howard J. W., 1995, ApJ, 438, 170
Holweger H., 2001, AIPC, 598, 23
Hoyos C., Díaz A. I. 2005, MNRAS, submitted
Izotov Y. L., Thuan T. X., 1998, ApJ, 500, 188
Izotov Y. L., Thuan T. X., Lipovetsky V. A., 1994, ApJ, 435, 647
Izotov Y. L., Thuan T. X., Lipovetsky V. A., 1997, ApJS, 108, 11
Jensen E. B., Strom K. M., Strom S. E., 1976, ApJ, 456, 504
Kennicutt R. C., Garnett D. R., 1996, ApJ, 456, 504
Kennicutt R. C., Bresolin F., French H., Martin P., 2000, ApJ, 537, 589
Kennicutt R. C., Bresolin F., Garnett D. R., 2003, ApJ, 591, 801
Kewley L. J., Dopita M. A., 2002, ApJS, 142, 35
Kinkel U., Rosa M. R., 1994, A&A, 282, 37
Kniazev A. Y., Pustilnik S. A., Ugryumov A. V., Pramsky A. G., 2001, A&A, 371, 404
Kobulnicky H. A., Kewley L. J., 2004, ApJ, 617, 240
Kobulnicky H. A., Kennicutt R. C., Jr, Pizagno J. L., 1999, ApJ, 514, 544
Kunth D., Sargent W. L. W., 1983, ApJ, 273, 81
Kwitter K. B., Aller L. H., 1981, MNRAS, 195, 939
Lequeux J., Rayo J. F., Serrano A., Peimbert M., Torres-Peimbert S., 1979, A&A, 80, 155
Lester D. F., Dinerstein H. L., Rank D. M., 1979, ApJ, 232, 139
Luridiana V., Peimbert M., Leitherer C., 1999, ApJ, 527, 110
McCall L. M., Rybski P. M., Shields G. A., 1985, ApJS, 57, 1
McGaugh S. S., 1991, ApJ, 380, 140 (McG91)
McGaugh S. S., 1994, ApJ, 426, 135
Monteverde M. I., Herrero A., Lennon D. J., 2000, ApJ, 545, 813
Nollenberg J. G., Skillman E. D., Garnett D. R., Dinerstein H. L., 2002, ApJ, 581, 1002
Oey M. S., Kennicutt R. C., 1993, ApJ, 411, 137
Oey M. S., Shields J. C., 2000, ApJ, 539, 687
Osterbrock D. E., 1989, Astrophysics of Gaseous Nebulae and Active Galactic Nuclei. San Francisco, Freeman
Pagel B. E. J., Edmunds M. G., Blackwell D. E., Chun M. S., Smith G., 1979, MNRAS, 189, 95
Pagel B. E. J., Edmunds M. G., Smith G., 1980, MNRAS, 193, 219
Pagel B. E. J., Simonson E. A., Terlevich R. J., Edmunds M. G., 1992, MNRAS, 255, 325
Pastoriza M. G., Dottori H. A., Terlevich E., Terlevich R., D'iaz A. I., 1993, MNRAS, 260, 177
Peimbert M., 1967, ApJ, 150, 825
Peimbert A., 2003, ApJ, 584, 735
Peimbert M., Peña M., Torres-Peimbert S., 1986, A&A, 158, 266
Peimbert A., Peimbert M., Luridiana V., 2002, ApJ, 565, 668
Pérez-Montero E., Díaz A. I., 2003, MNRAS, 346, 105 (PMD03)
Pettini M., Pagel B. E. J., 2004, MNRAS, 348, L59
Pilyugin L. S., 2000, A&A, 362, 325 (Pil00)
Pilyugin L. S., 2001a, A&A, 369, 594 (Pil01a)
Pilyugin L. S., 2001b, A&A, 373, 56
Popescu C. C., Hopp U., 2000, A&ASS, 142, 247
Rayo J. F., Peimbert M., Torres-Peimbet S., 1982, ApJ, 255, 1
Schaerer D., de Koter A., 1997, A&A, 322, 598
Scowen P. A., Dufour R. J., Hester J. J., 1992, AJ, 104, 92
Shaver P. A., McGee R. A., Danks A. C., Pottasch S. R., 1983, MNRAS, 204, 53
Shaw R. A., Dufour R. J., 1995, PASP, 107, 896
Shields G. A., Searle L., 1978, ApJ, 222, 281
Skillman E. D., 1989, ApJ, 347, 883 (S89)
Skillman E. D., Kennicutt R. C., 1993, ApJ, 411, 655
Skillman E. D., Kennicutt R. C., Jr, Hodge P. W., 1989, ApJ, 347, 875
Skillman E. D., Terlevich R. J., Kennicutt R. C., Jr, Garnett D., Terlevich E., 1994, ApJ, 431, 172
Skillman E. D., Côté S., Miller B. W., 2003, AJ, 125, 593
Stasińska G., Leitherer C., 1996, ApJS, 107, 661
Storchi-Bergmann T., Calzetti D., Kinney A. L., 1994, ApJ, 429, 572
Storchi-Bergmann T., Schmitt H.R., Calzetti D., Kinney A. L., 1998, AJ, 115, 909
Tayal S. S., Gupta G. P., 1999, ApJ, 526, 541
Terlevich R. Melnick J., Masegosa J., Moles M., Copetti M. V. F., 1991, A&AS, 91, 285
Urbaneja M. A., Herrero A., Bresolin F., Kudritzki R.-P., Gieren W., Puls J., 2003, ApJ, 584L, 73
Van Zee L., Skillman E. D., Salzer J. J., 1998, AJ, 116, 1186
Vermeij R., Damour J. M., van der Hulst J. M., Baluteau J.-P., 2002, A&A, 390, 649
Vila-Costas M. B., Edmunds M. G., 1992, MNRAS, 259, 121
Vílchez J. M., Esteban C., 1996, MNRAS, 280, 720
Vílchez J. M., Iglesias-Páramo J., 2003, ApJS, 145, 225
Vílchez J. M., Pagel B. E. J., Díaz A. I., Terlevich E., Edmunds M. G., 1988, MNRAS, 235, 633
Zaritsky D., 1992, ApJ, 390, 732
Zaritsky D., Kennicutt R. C., Jr, Huchra J. P., 1994, ApJ, 420, 87 (ZKH94)

SUPPLEMENTARY MATERIAL

The following supplementary material is available for this article online.

Table 2. Recalculated electron densities of [S II], electron temperatures of [O II] and [O III] and ionic abundances of O^+ and O^{2+} for the whole sample.

This paper has been typeset from a TEX/LATEX file prepared by the author.